Nucleic Acids Research, 2025, **53**, gkae1189
https://doi.org/10.1093/nar/gkae1189
Synthetic Biology and Bioengineering

Engineering oxypurinol-responsive riboswitches based on bacterial xanthine aptamers for gene expression control in mammalian cell culture

Vera Hedwig[1,2], Maike Spöring[1,2], Julia Ottlinger[1], Sila Köse[1,2], Herbert Nar[3], Gisela Schnapp[3], Dirk Gottschling[3], Holger Klein[4], Gary Aspnes[3], Matthias Klugmann[5] and Jörg S. Hartig[1,2,*]

[1]Department of Chemistry, University of Konstanz, Konstanz, Germany
[2]Konstanz Research School Chemical Biology (KoRS-CB), University of Konstanz, Konstanz, Germany
[3]Medicinal Chemistry, Boehringer Ingelheim Pharma GmbH & Co. KG, Biberach an der Riss, Germany
[4]Global Computational Biology and Digital Sciences, Boehringer Ingelheim Pharma GmbH & Co. KG, Biberach an der Riss, Germany
[5]Research Beyond Borders, Boehringer Ingelheim Pharma GmbH & Co. KG, Biberach an der Riss, Germany
[*]To whom correspondence should be addressed: Tel: +49 7531 88 4575; Email: joerg.hartig@uni-konstanz.de

Abstract

Riboswitch-mediated control of gene expression without the interference of potentially immunogenic proteins is a promising approach for the development of tailor-made tools for biological research and the advancement of gene therapies. However, the current selection of applicable ligands for synthetic riboswitches is limited and strategies have mostly relied on de novo selection of aptamers. Here, we show that the bacterial xanthine I riboswitch aptamer recognizes oxypurinol, the active metabolite of the widely prescribed anti-gout drug allopurinol (Zyloprim®). We have characterized the aptamer/oxypurinol interaction and present a crystal structure of the oxypurinol-bound aptamer, revealing a binding mode similar to that of the cognate ligand xanthine. We then constructed artificial oxypurinol-responsive riboswitches that showed functionality in human cells. By optimizing splicing-based oxypurinol riboswitches using three different strategies, transgene expression could be induced by >100-fold. In summary, we have developed recombinant RNA switches enabling on-demand regulation of gene expression in response to an established and safe drug.

Graphical abstract

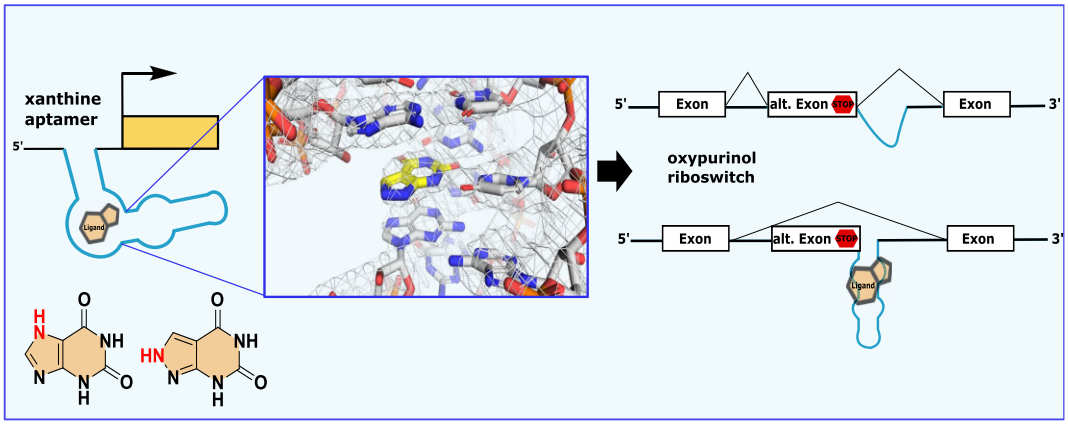

Introduction

Riboswitches allow ligand-dependent induction or inhibition of gene expression by RNA-only mechanisms (1). Since these systems do not rely on the presence of regulatory proteins, they display several advantages such as decreased immunogenicity, a smaller genetic footstep and more robust control of gene expression which are key features for next generation gene therapy applications (2,3). A large number of natural riboswitch classes binding a variety of ligands have been found to control gene expression mostly in bacteria (1). While the expression platforms that ultimately carry out the regulation vary in a modular fashion, the ligand-sensing aptamer domains are highly conserved even between only distantly related species (4,5). Artificial riboswitches have been

Received: May 15, 2024. **Revised:** September 24, 2024. **Editorial Decision:** October 24, 2024. **Accepted:** February 19, 2025

developed to control transgene expression not only in bacteria but also in several eukaryotic model organisms (6–11). As with their natural counterparts, different artificial expression platforms can be combined with ligand-sensing aptamers, providing a certain degree of modularity. Most artificial systems include *de novo*-generated ligand sensors such as the cb32-minimer variant of the tetracycline-binding aptamer (12–14). It has been shown that artificial riboswitches are suitable to regulate recombinant adeno-associated virus (AAV)-mediated transgene expression in mice, potentially improving safety and precision of gene therapy (3,15–20). However, the repertoire of efficient riboswitches binding therapeutically relevant ligands is currently limited to very few compounds such as tetracycline (12,21,22). Although bacterial purine-binding aptamer sequences have been implemented successfully in artificial riboswitch constructs and are functional in human cells, *in vitro*-selected aptamers are still most commonly used for synthetic designs (22–27).

Natural aptamers bind their respective ligands with high affinity and specificity. However, structurally similar compounds or derivatives have sometimes been shown to activate riboswitches (28,29). In 2020, Breaker and coworkers identified the bacterial NMT1 RNA motif as a riboswitch responsive to xanthine, later naming it the xanthine I riboswitch (30–32). The NMT1 motif is present in several bacterial species in the UTR of genes potentially involved in purine degradation, such as the tauA gene from *Serratia plymuthica* (*S. plymuthica*). The characterization by Yu *et al*. has been carried out with this tauA sequence of the xanthine riboswitch (30). In addition to its name-giving ligand, the xanthine I riboswitch also responds to 8-azaxanthin and to a lesser extent to uric acid. By solving the crystal structure of a modified tauA xanthine I aptamer in complex with xanthine, Xu *et al.* gained insight into the structural basis for ligand recognition of this riboswitch (33). It consists of a hairpin-like structure with two stems (P1 and P2), separated by two junctions (J1 and J2). The ligand is bound between J1, J2 and P1, coordinated by three Mg^{2+} ions and inserts between the A6 and G35 nucleobases to form pi-stacking interactions.

During the mammalian purine salvage pathway, xanthine is generated and converted by xanthine oxidase to uric acid, which is in turn eliminated via the renal system (34). Since higher primates lack uricase responsible for further degrading uric acid, human uric acid levels are higher than in most mammals, which is one reason for the development of hyperuricaemia (35). A commonly used treatment of hyperuricemia is the administration of allopurinol (Zyloprim®, Caplenal®, Zyloric® and others). In humans allopurinol has a short half-life ($t_{\frac{1}{2}} \sim 1$h) and is rapidly metabolized to oxypurinol by xanthine oxidase (Supplementary Scheme 1) (36). Oxypurinol inhibits xanthine oxidase and thereby reduces uric acid formation (37). Allopurinol was prescribed for treatment of hyperuricemia over 15 million times in the US in 2021 (ranked 40th on the list of most prescribed drugs) and is included on the WHO list of essential medicines (38,39).

We show herein that the xanthine I aptamer can be utilized to engineer an artificial riboswitch that is triggered by oxypurinol. We show that oxypurinol binds to the xanthine I aptamer with an increased K_d of 15.8 μM, compared to a K_d of 3.3 μM for the physiological ligand xanthine. A crystal structure of the oxypurinol-bound xanthine aptamer gives insights into the molecular basis of this interaction. We then show that the xanthine aptamer is well suited for the generation of artificial riboswitches based on different expression platforms in mammalian cells. Attachment of the aptamer sequence to Hammerhead (HHR) ribozymes results in off-switches, while the regulation of splice site accessibility of an alternative exon generates on-switches. Finally, these on-switches were optimized via new design strategies such as the addition of alternative stem structures, additional binding sites and splicing-modulating quadruplex sequences, ultimately yielding synthetic RNA switches with up to 130-fold induction of gene expression by oxypurinol in human cell culture.

Materials and methods

In-line probing

The xanthine aptamer sequence was amplified with a T7 promotor and a 20 nt hairpin sequence for improved visualization of the relevant bases. After PAGE-Gel purification, ∼80 pmol of RNA was dephosphorylated with Shrimp Alkaline Phosphatase (NEB), labeled with [γ-32P]-ATP (Hartmann Analytic) and PAGE-purified. In-line probings were performed as previously described (40,41). [γ-^{32}P]-labeled RNA was incubated with 20 mM $MgCl_2$, 100 mM KCl and 50 mM Tris–HCl (pH 8.3) and the ligand or 2% DMSO. Ligands (xanthine and oxypurinol) dissolved in 100% DMSO (250 mM ligand concentration), resulting in a maximum concentration of 2% DMSO using 1 μl at the 10 μl in-line probing reaction with the highest ligand concentration. The RNA fragments were separated on a denaturing 8% PAGE-gel. The band pattern was visualized in a phosphorimager (GE Healthcare Life Sciences) and analyzed using Quantity One. The change in the band intensity of G33 and A6 was quantified and normalized to the band intensity corresponding to G14. Data points were analyzed by a sigmoidal dose-response fit, setting the lowest value as 0 and the highest value as 1.

Plasmid construction

The riboswitch sequences were inserted into psiCHECK-2 vectors, encoding Renilla luciferase (hRluc) and firefly luciferase (hluc+) via overhang extension PCR. The cassette exon for splicing-based riboswitch design was inserted as previously described (42). The exon-skipping switches were modulating hluc + expression, while hRluc expression served for transfection control. The splicing-cassette was inserted in an mCherry/EGFP reporter via Gibson-Assembly (see Supplementary Table S5 for primer sequences). In this design, the switches were modulating mCherry expression, while EGFP served as transfection control. Aptazyme off-switches were inserted into the 3′-UTR of hRluc and hluc + served as internal control. All oligonucleotides were ordered from Sigma-Aldrich. Plasmids were purified using a Zyppy Plasmid Miniprep kit (Zymo Research).

Cell culture experiments

All cell lines were cultivated in Dulbecco's modified Eagle's medium (Gibco DMEM, Fisher Scientific) supplemented with 10% (v/v) fetal calf serum and1% (v/v) penicillin/streptomycin (Fisher Scientific) at 37°C in 5% CO_2 humidified atmosphere. 24 h before plasmid transfection, 15 000 cells were seeded in 96-well plates. For transient transfection, a Lipofectamine3000 kit (Thermo Fisher Scientific) was used. Three wells were transfected for each condition and construct, using 100 ng plasmid DNA per transfection. After

incubation of 4 h at 37°C, the medium was replaced by Dulbecco's modified Eagle's medium (Gibco DMEM, Fisher Scientific) with oxypurinol dissolved in 1 M NaOH (200 mM stock concentration, resulting in a 1:100 dilution for the preparation of a 2 mM oxypurinol sample, followed by neutralization with 1 M HCl). Xanthine, Azaxanthine, Hypoxanthine and Allopurinol were dissolved in 1M NaOH to a final stock concentration of 100 mM. When applying uric acid, a new dilution in 1M NaOH (final uric acid concentration of 50 mM) was prepared prior to each experiment and used immediately. After addition of the ligands to the medium, HCl was added for neutralization. Controls were treated with Dulbecco's modified Eagle's medium, supplemented with 1 M NaOH and 1 M HCl.

Dual luciferase assay

Twenty-four hours after transfection, luciferase expression cells were measured using the Dual-Luciferase Reporter Assay System (Promega) according to the manufacturer's protocol. The luminescence was quantified with a Spark multimode microplate reader (Tecan), applying a settling time of 0 ms and an integration time of 2000 ms.

Fluorescence reporter assay

Cells were transfected with plasmids carrying the mCherry/GFP constructs using a Lipofectamine3000 kit (Thermo Fisher Scientific). 4 h post-transfection, the medium was replaced as described above. Due to high background fluorescence, untransfected cells were treated with medium with or without oxypurinol. After twenty hours of incubation, cells were washed with PBS, covered with 100 µl PBS and the fluorescence was detected with a Spark multimode microplate reader (Tecan). The background values for EGFP and mCherry were measured from non-transfected cells and subtracted from all constructs prior to normalization.

RT-PCR and qPCR analysis

To evaluate the regulation of the riboswitches on the RNA level, HeLa cells were transfected with the best-performing construct (SP_double_anti_GQ) as well as the psiCheck plasmid without any riboswitch and a plasmid that contains the splicing-cassette in the firefly gene and incubated the cells for 24 h in absence and presence of 2 mM oxypurinol. RNA from the transfected cells was purified and then used for RT-PCR with primers binding downstream and upstream of the alternative exon as the previously described visualization of the splicing pattern by Finke *et al.* (42) RNA extraction was performed using the Quick-RNA™ Miniprep Kit (Zymo Research) according to the manufacturer's instructions. To remove any residual DNA, an additional DNaseI treatment (Thermo Scientific™) was carried out, followed by RNA purification using the RNA Clean & Concentrator-100 kit (Zymo Research). A total of 500 ng of purified RNA was then reverse transcribed using random hexamers and the High Capacity cDNA Reverse Transcription Kit (Applied Biosystems) following the protocol (10 min at 25°C, 120 min at 37°C, 5 min at 85°C). For PCR, 1 µl of the resulting cDNA was amplified (see Supplementary Table S5 for primer sequences) using Phusion Plus polymerase (New England Biolabs) with an initial denaturation at 98°C for 30 s, followed by 30 cycles of 98°C for 10 s, 60°C for 30 s and 72°C for 20 s, with a final elongation step at 72°C for 7 min. The amplified product was analyzed on a 2% (w/v) agarose gel.

We further performed a qPCR as described by Finke *et al.* (42) using primers that bind exclusively to exon 1 to quantify the firefly luciferase mRNA levels (see Supplementary Table S5 for primer sequences), previously designed and used by Beilstein *et al.* and Finke *et al.* (7,42) To confirm qPCR specificity, we verified appearance of single peaks in the melt curve analysis and visualized the amplicons as single bands of the expected size on a 2% agarose gel. Cq values were determined using Bio-Rad CFX Maestro 1.1 software. No-template controls were included and each sample was run in technical duplicates. Data were analyzed using the delta-Cq method with hRluc as the reference gene and mean mRNA levels were calculated from three independent experiments.

Resazurin assay

HeLa cells were seeded in a 96-well plate (~15 000 cells/well). After 24 h of incubation, the medium was replaced by medium containing the ligands (oxypurinol, xanthine, azaxanthine, hypoxanthine, at concentrations between 5 and 0.125 mM. Controls with medium (set to 100% viability), medium supplemented with 1 M NaOH and 1 M HCl and medium containing 5% Triton X-100 (negative control) were added to the plate. 24 h after ligand addition, the medium was replaced by resazurin containing medium (1:10 dilution in medium, using a 0.55% (w/v) stock solution), followed by an incubation time of 1 h. Fluorescence of resorufin was measured at a Spark® multimode microplate reader (Tecan) (Excitation: 530 nm, Emission: 590 nm). All resazurin assays were performed in three individual experiments with technical triplicates.

Statistical analysis

Statistical analysis was performed in Python 3.12.4 using scipy.stats 1.13.1 package. *P* values were determined by a one-way analysis of variance (ANOVA).

Isothermal titration calorimetry (ITC)

Isothermal titration calorimetry experiments were conducted with a PEAQ ITC instrument (Malvern). 53 tauA or NMT1 RNA were buffer exchanged with protein desalting spin columns (nThermo Scientific, cat #89849) equilibrated in 10 mM Tris pH 7.5, 10 mM KCl, 5 mM $MgCl_2$. Complete saturation of 20 µM RNA was typically achieved by injecting 18 × 2 µl aliquots of 250 µM Oxypurinol or Xanthin at 25°C. The thermodynamic binding parameters were extracted by nonlinear regression analysis of the binding isotherms (PEAQ ITC software, Malvern). A single-site binding model was applied yielding the binding enthalpy (ΔH), stoichiometry (n), entropy (ΔS) and association constant (K_a). At least two independent experiments were performed. A table with the results is shown in Supplementary Table S3.

Crystallisation and crystal structure determination

Xanthine I riboswitch aptamer RNA (sequence 5′-GGAGUAGAAG CGUUCAGCGGCCGAAAGGCCGC CCGGAAAUUGCUCC-3′) was synthesized at Axolabs GmbH (Kulmbach, Germany) and subsequently purified by HPCL. Crystals were obtained with xanthine aptamer RNA in the presence of either xanthine or oxypurinol. RNA was

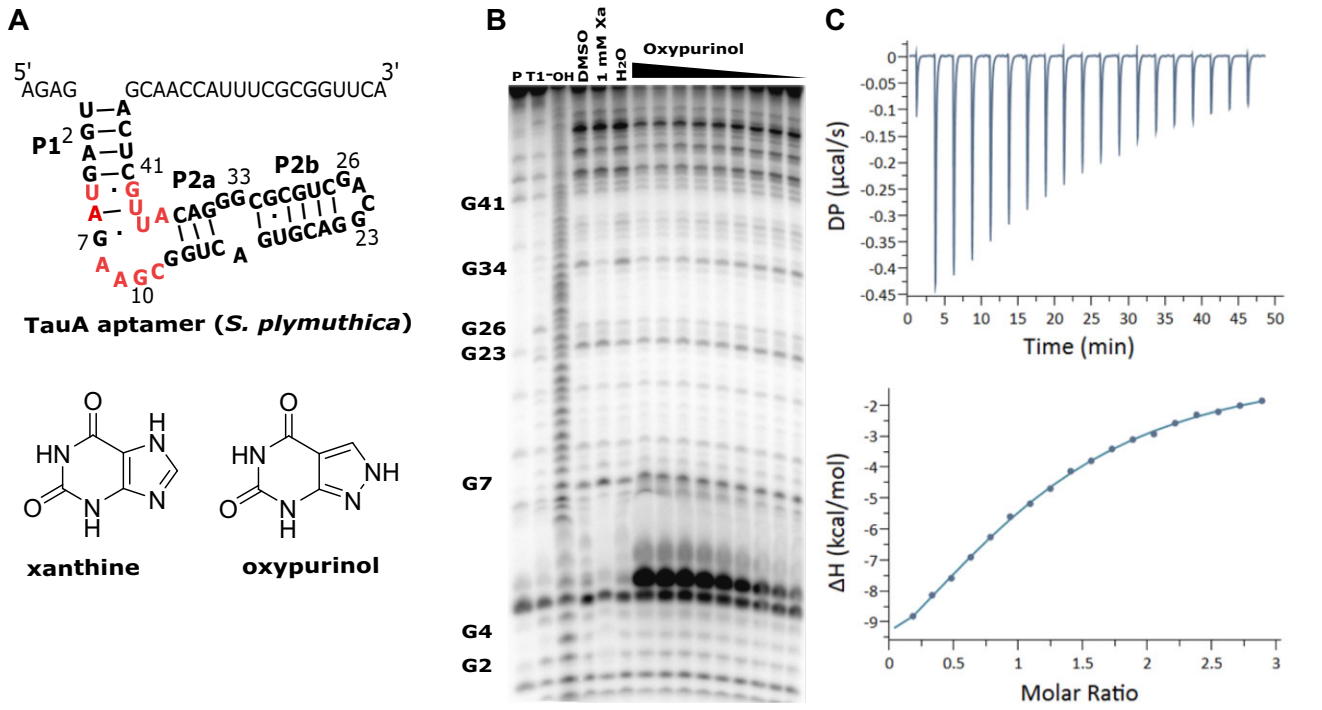

Figure 1. The tauA xanthine aptamer from *S. plymuthica* motif RNA binds oxypurinol. (**A**) Sequence and secondary structure of the xanthine I aptamer from *S. plymuthica*, numbering according to the '68 construct' studied by Yu *et al.* (30). (**B**) PAGE gel analysis of an in-line probing reaction of 5′-^{32}P-labeled xanthine aptamer from *S. plymuthica* S13 with DMSO, 1 mM xanthine (Xa), H_2O and oxypurinol 1:2 dilutions from 5 to 19.5 µM. Untreated 5′-^{32}P-labeled RNA (precursor, P), T1 RNase (T1) digested or alkaline digestion (OH^-) serve as controls. (**C**) Titration of oxypurinol (300 µM) in 20 µM TauA aptamer RNA containing 53 nt of the upstream TauA sequence from *S. plymuthica* (30).

dissolved in water at a concentration of 1.4 mM and diluted to 400 µM in buffer containing 50 mM HEPES, pH 7.0, 50 mM KCl, 5 mM $MgCl_2$. RNA was annealed by first heating the sample for 5 min at 65°C before cooling on ice for 30 min. Ligands were dissolved in 10 mM sodium hydroxide and added to RNA at a concentration of 6 mM. The RNA and ligand mixture was incubated for 90 min on ice. Prior to setting up crystallization trays the solution was centrifuged for 10 min at 130 000 rpm at 4°C. Crystallization was carried out in sitting drop format. Droplets were set up using a Mosquito pipetting robot. 150 nl drops were pipetted using RNA to reservoir volume ratios of 2:1, 1:1 and 1:2. Crystals grew under various conditions. The xanthin co-crystals used for structure determination grew in 12% 2-propanol, 0.2 M calcium acetate, 0.1 M MES at pH 5.8 and 20°C. Oxypurinol co-crystals grew in 0.1 M ammonium sulfate, 0.1 M sodium chloride, 20% PEG 8000, 1 M sodium formate, 50 mM Bis–Tris pH 7 and 4°C. Crystals were flash frozen in liquid nitrogen after addition of 30% glycerol to the mother liquor. Data were collected at the Swiss Light Source (SLS, Villigen) on beamline PX2 and processed using XDS. The structures were solved using molecular replacement (Phaser) with 7elr (33) as the starting model. Model building was done in Coot (43) and structures were refined with autoBUSTER (44).

Results

The bacterial xanthine-I riboswitch aptamer binds oxypurinol

Due to their structural similarity, we hypothesized that oxypurinol could also bind to the bacterial xanthine I riboswitch. To address this hypothesis, we analyzed the TauA motif from *S. plymuthica* (30) in presence of xanthine and oxypurinol via an in-line probing reaction and visualized the resulting RNA fragments on a PAGE gel (Figure 1A, B). The addition of oxypurinol exhibited a pronounced RNA/ligand interaction and caused a surprisingly strong increase in the band intensities at positions 4–10 with A6 being the most prominent cleavage site. The bands at position 34 and 44–46 decreased in a similar fashion as with the addition of the natural ligand xanthine. Binding of oxypurinol seems to reorganize the ribose and phosphodiester moieties at and around position A6 into a conformation most favorable for in-line attack, resulting in the drastically increased intensity of the corresponding bands on the PAGE gel (Figure 1B). Quantification of the relative intensities of A6 and G34 results in a K_d of ∼236 and 388 µM, respectively (Supplementary Figure S1). Isothermal titration calorimetry (ITC) confirmed oxypurinol binding and determined the binding thermodynamics (Figure 1C and Supplementary Table S3). Analysis of the resulting data sets suggests 4.8-fold reduced affinity of the aptamer for oxypurinol (K_d = 15.8 ± 0.4 µM) compared to xanthine (K_d = 3.29 ± 0.17 µM) (Supplementary Figure S2 and Supplementary Table S3). The differences in the affinities obtained by in-line probing analysis may be a result of the substantial RNA cleavage at position A6 causing an overall reduction in the longer RNA fragments.

Crystal structure of the aptamer-oxypurinol complex

To elucidate the structural basis for oxypurinol binding by the xanthine I aptamer, we solved co-crystal structures for both xanthine and oxypurinol in complex with the aptamer.

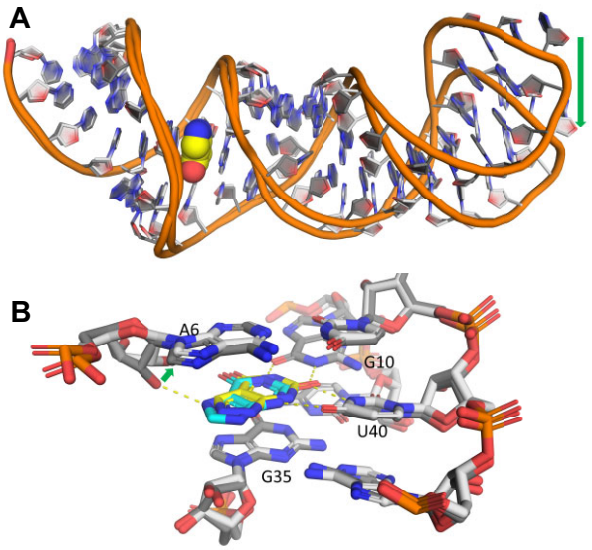

Figure 2. Co-crystal structure of the xanthine aptamer and oxypurinol. (**A**) Superposition of the xanthin-bound 1 structure and the xanthin-bound 2/oxypurinol-bound structure. A significant, crystal packing induced shift of the tip region (G23–G27) is observed (green arrow). (**B**) Oxypurinol (yellow carbon atoms, corresponding RNA structure with light grey carbon atoms) is bound in a very similar fashion to xanthine (cyan carbon atoms, corresponding RNA structure with dark grey carbon atoms, superposition of 7elr with the oxypurinol co-structure reported herein). Overall structure, fold and interactions of shown positions with the neighboring nucleobases are conserved. The hydrogen bond to the C2′-hydroxyl of the A6 ribose (dashed yellow line) is disrupted in the complex with oxypurinol, resulting in a different conformation of the A6 ribose and phosphodiester moieties (green arrow).

Crystals obtained from the RNA-xanthin complex were isomorphous to the co-crystals described before (33). Our crystals diffracted up to 2.0 Å resolution, however, with a relatively strong diffraction anisotropy (3.0 and 2.4 Å in *b* and *c* direction of the orthorhombic crystals) (Supplementary Table S4). Structural findings were identical to the ones described by Xu *et al.*, including the geometry of the ligand binding site. A second crystal form was obtained with a related but distinct space group which contains one RNA complex in the asymmetric unit and is more loosely packed and hence diffracted to only lower resolution. Crystals of the oxypurinol complex were obtained under identical conditions to the second crystal form of xanthine/aptamer RNA co-crystals (Supplementary Table S4). The crystals are of space group *I*222 with cell constants $a = 72.8$ Å, $b = 85.1$ Å, $c = 97.2$ Å and diffracted to 2.6 Å resolution, again with a strong anisotropic behavior (3.0 Å in the other two crystal dimensions). Comparison of the xanthine- and oxypurinol-bound structures show an overall highly conserved fold (Figure 2). The largest deviations are found in the loop region comprising G23–G27, which appears to be more flexible relative to the other parts of the aptamer structure. Due to the crystal anisotropy, lower overall resolution and a high Wilson B-factor, the ligand environment could not be resolved to a similar level of detail compared to the xanthine co-structure (Supplementary Figure S3). In particular, it was not possible to model the hydration environment and magnesium ions. However, it is evident that oxypurinol binds to the xanthine binding site of the aptamer forming very similar hydrogen bonding interactions with the adjacent nucleobases G10 and U40 and stacking interactions with A6 and G35. The N7 nitrogen shifted to the 8-position in oxypurinol leads to a disruption of the N7 hydrogen bond with the C2'-hydroxyl group of the A6 ribose that is found in the xanthine-RNA complex. Superposition of the two structures shows a slight lateral shift by 0.5 Å of oxypurinol relative to xanthine and a shift of the C2'-hydroxyl group to avoid an unfavorable proximity of the hydroxyl and the C7-H. Loss of this ligand-RNA hydrogen bond is consistent with the observed five-fold reduction of binding affinity of oxypurinol versus xanthine (45). The changed position of the C2′-hydroxyl group and the likely increased flexibility resulting from the lack of the hydroxyl/ligand H-bond explains the observation of the drastically increased cleavage of the phosphodiester bond at and around position A6 in the in-line probing experiment shown in Figure 1.

Design of artificial ribozyme- and exon-skipping riboswitches with tauA aptamers

To exploit the possibility to bind to and potentially trigger artificial RNA switches with the xanthine analog oxypurinol or its precursor drug allopurinol, we next examined whether controlled gene expression in mammalian cells can be achieved by utilizing the xanthine aptamer sequence as ligand-sensing domain. Artificial riboswitches have been reported to be modular with regards to an exchange of the ligand sensing aptamer domains (8,24,46,47). To determine whether the xanthine I aptamer can be utilized as a ligand sensing domain on riboswitch platforms for controlling transgene expression in human cells, we connected the xanthine I aptamer via stem I to a type I hammerhead ribozyme (HHR) (24,48), which resulted in 3-fold off-switches (Supplementary Figure S4 and Supplementary Note 1). While this result demonstrates the utility of the bacterial riboswitch derived xanthine I aptamer in constructing RNA-based genetic switches in a human cell line, mM range concentrations of oxypurinol were necessary to achieve this modest level of suppression. Based on this result we turned our attention to the design of on-switches as these are preferred for most applications and offered the prospect of improved response to the effector.

In order to construct synthetic oxypurinol-responsive riboswitches with improved properties we re-engineered switches based on an expression platform that relies on ligand-dependent exon skipping. In the past we have used such designs for the construction of efficient tetracycline-dependent on-switches (42). The design of the expression platform comprises two introns surrounding an alternative exon that contains a premature stop codon that results in inhibited gene expression in absence of the effector (49). The aptamer is placed between the 5′-splice site and a complementary anti-splice site, resulting in the formation of a stable stem upon ligand binding. Masking of the 5′-splice site in presence of the ligand provokes exon skipping and induces gene expression (Supplementary Figure S5). We incorporated xanthine aptamers from different bacterial species into the regulatory cassette to evaluate sequence characteristics that are necessary for a functional switch in this context (Supplementary Note 2). In this context, four out of five tested xanthine aptamers led to oxypurinol-inducible on-switches. The most effective switches displayed dynamic ranges of ∼3-fold and were obtained with the aptamer of *S. plymuthica* and *Inquilinus limosus (I. limosus)* (Supplementary Figure S5, Supplementary Table S1 and

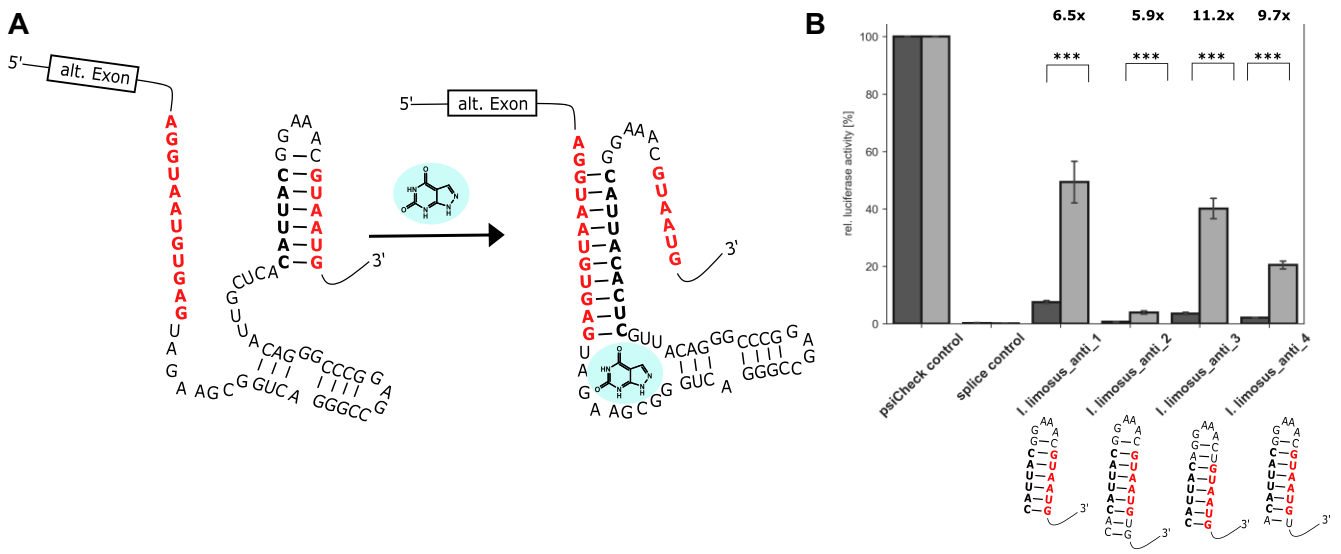

Figure 3. Improving riboswitch performance by addition of a competing stem. (**A**) Scheme of the splicing-based riboswitch design including a stem that competes with aptamer formation and thereby ameliorates the splice site accessibility. (**B**) Luciferase expression after transfection of HeLa cells with riboswitches harboring the aptamer sequence of *I. limosus* and competing stems in absence (dark grey) or presence (light grey) of 2 mM oxypurinol. Bar plots show the mean (±SD) of three independent replicates, each measured in triplicates $*P < 0.05$, $**P < 0.01$, $***P < 0.001$.

Supplementary Table S2). Taken together, we demonstrated that bacterial xanthine aptamers are suited to construct synthetic RNA switches in human cells responding to oxypurinol employing both ribozymes and exon-skipping as expression platforms.

Improving exon-skipping oxypurinol riboswitches

The riboswitches based on xanthine I aptamers from *S. plymuthica* and *I. limosus* display a high level of gene expression in presence of oxypurinol, however, high background expression in absence of the ligand limits their switching performance. We thus aimed for an improved design that would prevent aptamer formation and masking of the splice site in the ligand unbound state. A common mechanism in natural riboswitches from bacteria is the formation of a terminator stem that competes with the folding of the aptamer, leading to the regulation of gene expression via antitermination in response to ligand binding (50). We hypothesized that such an additional stem could help to balance out the two anticipated folds in absence and presence of the ligand.

To determine whether a rationally devised competing stem is effective in our context to diminish unintended splice site masking in absence of the ligand, we positioned additional stem-loop sequences downstream of the aptamer. These anti-stem sequences are designed to be partially complementary to the anti-splice site to allow the mutually exclusive formation of a stable stem and release of the splice site in absence of the ligand, while aptamer formation should be favored in presence of the ligand (Figure 3A). To improve the design of the structure, base pairs were inserted at both ends of the stem sequence, either adding to the part that reaches into the aptamer sequence or elongating the stem (for details, see Supplementary Note 3 and Supplementary Figure S6). Increased interference with the aptamer sequence leads to the lowest level of gene expression, whereas elongation of the stem loop results in less pronounced effects. With this, we were able to design more efficient on-switches with lower background expression and up to 11-fold dynamic range (Figure 3B).

Partial folding of the aptamer and formation of the splice site-masking stem P1 in absence of the ligand causes background gene expression, which was decreased by the introduction of an additional stem, however, as it competes with aptamer folding, the on-state is also affected. Next, we fused stem P2 to a second xanthine I aptamer in order to decrease the probability of aptamer folding without induction (for details, see Supplementary Note 4 and Supplementary Figure S7). In presence of the ligand, folding of the second aptamer should allow P2 formation, followed by ligand binding and folding of the first aptamer, thereby creating cooperativity between both binding pockets. The best-performing riboswitch with fused aptamers (I. limosus_double_4) has a similar low background expression of ∼10% but an unaffected on-state of 130 %, causing an improvement of the dynamic range to 13-fold (Figure 4A, B).

Comparing the effects of aptamer fusion and anti-stem insertion for optimization of the riboswitches, we found that the incorporation of a competing strand provided the most efficient background reduction. The fusion of two aptamers resulted in a moderate decrease in background expression while maintaining a high on-state, which led to an increased disparity in the level of gene expression between the induced and non-induced states. To make use of both effects, we decided to combine the designs by fusing the best-performing anti-stem constructs with a second aptamer (Figure 5). The additional reduction of the background and the increased difference between on-and off-level led to a strong improvement of the dynamic range. Combination of the I. limosus_anti_1 construct with the I. limosus_double_4 design (IL_double_anti_2) results in a fold-change of 36-fold. Adding a second aptamer from *S. plymuthica* to the anti-stem design (SP_double_anti) further reduces the background causing a dynamic range of > 40-fold. Mutating the binding

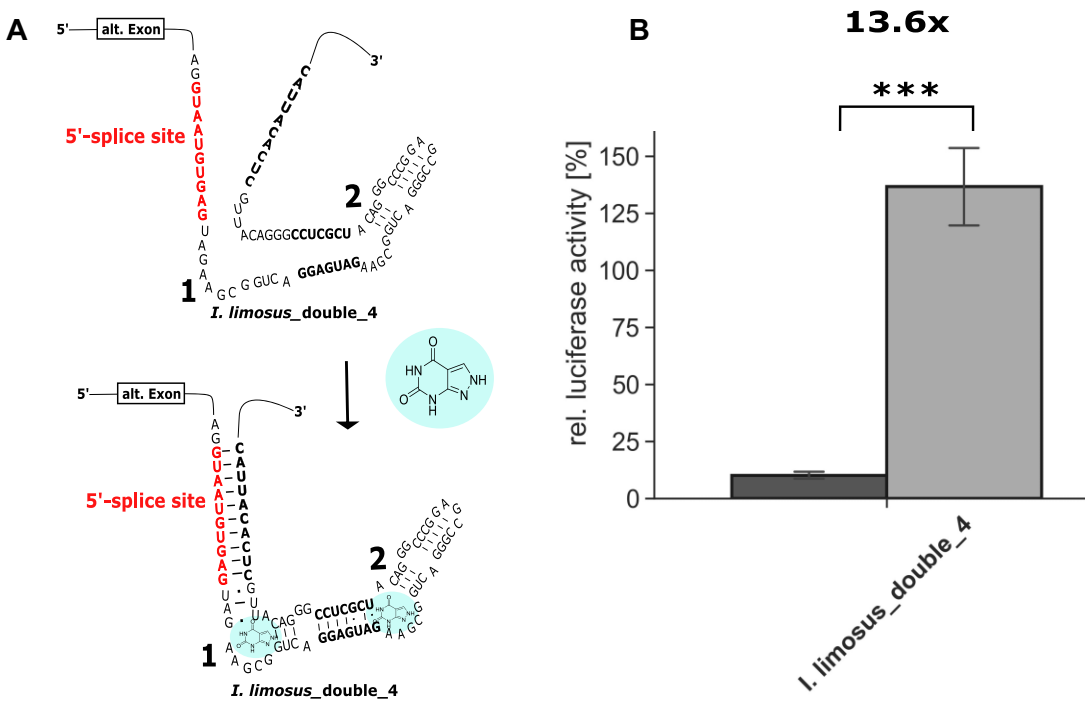

Figure 4. Improved riboswitch performance by implementation of two aptamers. (**A**) Schematic depiction of the predicted secondary structure of a fusion of two xanthine I aptamers from *I. limosus* (I. limosus_double) in the riboswitch construct in absence and presence of oxypurinol. (**B**) Relative luciferase expression of Hela cells after transfection with riboswitches containing fused aptamer structures with a connection stem of variable length and sequence in absence (dark grey) or presence (light grey) of 2 mM oxypurinol. Relative luciferase expression was normalized to a control vector containing an unmodified luciferase gene (psiCheck control). Shown is the mean (±SD) of three independent experiments, performed in triplicates $^{**}P < 0.01$, $^{***}P < 0.001$.

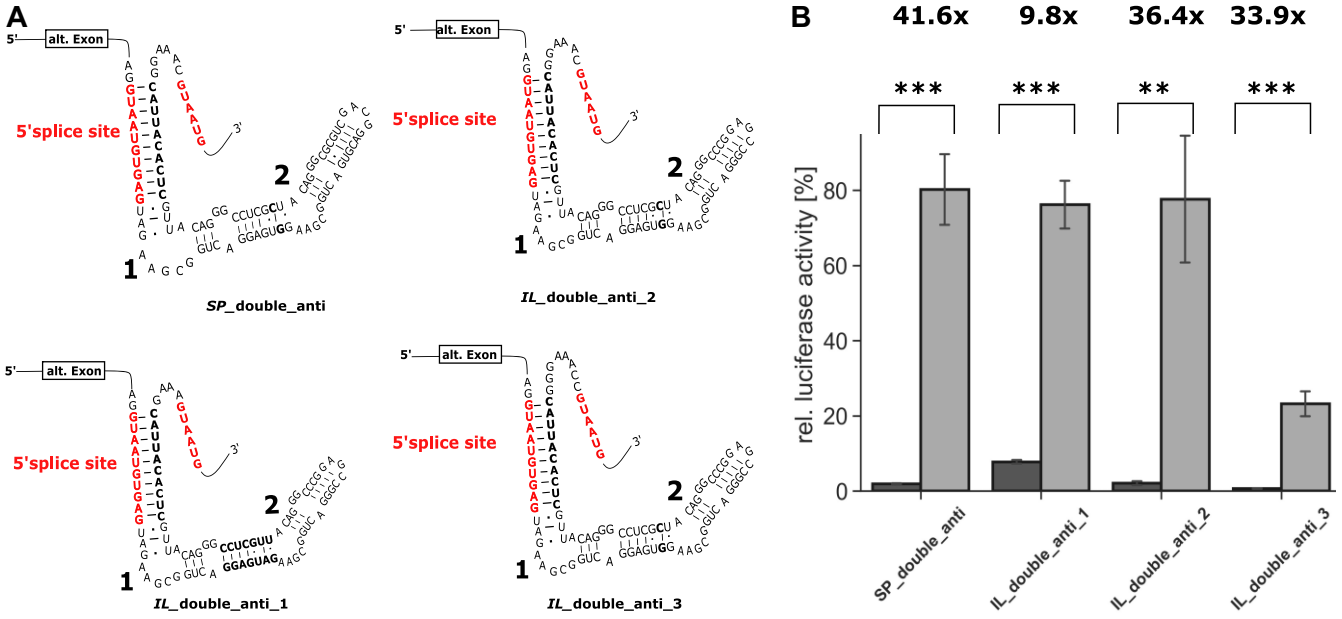

Figure 5. Improvement of switching performance by combination of fused aptamers with competing stems. (**A**) Sequence of fused aptamers from *S. plymuthica* (SP_double_anti) and *I. limosus* (IL_double_anti) in combination with competing stems. (**B**) Luciferase expression of Hela cells transfected with riboswitches containing the fused aptamers and competing stems in absence (dark grey) or presence (light grey) of 2 mM oxypurinol. Bars represent the mean (±SD) of three independent experiments, performed in triplicates $^{**}P < 0.01$, $^{***}P < 0.001$.

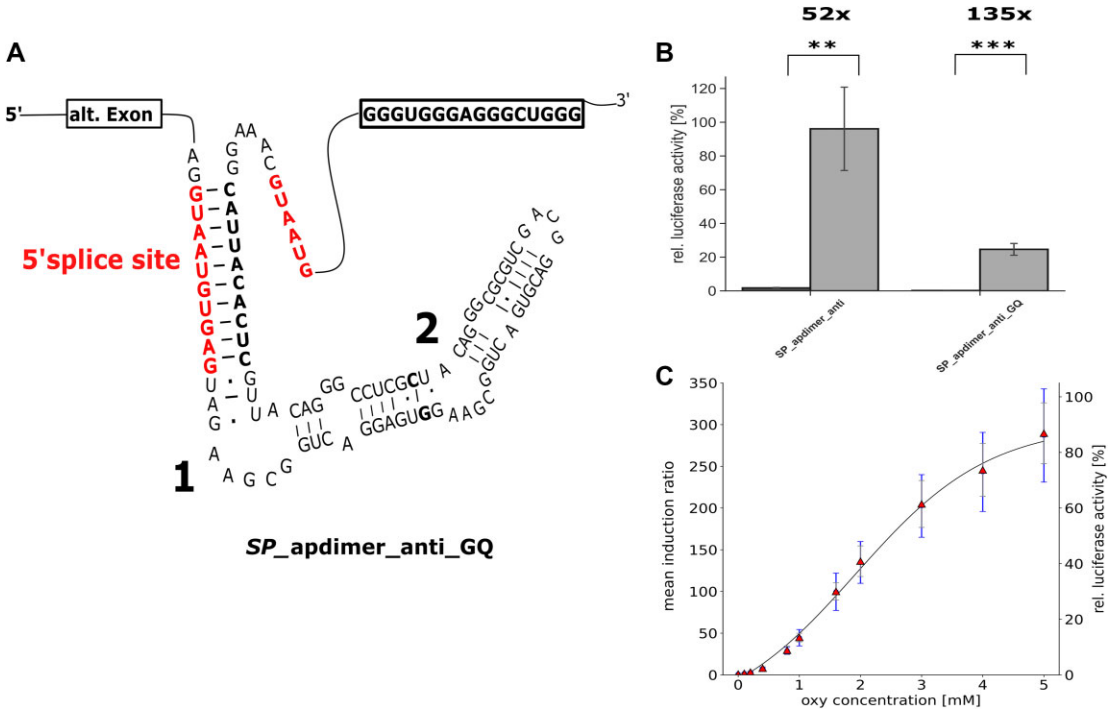

Figure 6. Improvement of switching performance by incorporation of a G-quadruplex sequence and ligand selectivity (**A**) Sequence and predicted secondary structure of the SP_double _anti construct with inserted G-quadruplex (SP_double_anti_GQ) 18 nt downstream of the riboswitch element. (**B**) Luciferase expression of HeLa cells transfected with constructs containing the SP_double_anti riboswitches with and without G-quadruplex sequence in absence (dark grey) or presence (light grey) of 2 mM oxypurinol. Bars represent the mean (±SD) of three independent experiments, performed in triplicates. ***$P < 0.001$. (**C**) Concentration-dependent increase in fold change and luciferase activity of the SP_double_anti_GQ construct. Data points show the mean of three individual replicates(±SD fold in blue and ± SD rel.luc acitivity in grey), each performed in triplicates.

sides of the SP_double_anti switch indicates that both pockets are contributing to the improved switching-performance (Supplementary Figure S8 and Supplementary Note 5).

Next, we wanted to optimize splicing of the alternative exon in the uninduced state to minimize leakiness in absence of the ligand. Introduction of an intronic G-quadruplex adjacent to the 5′-splice site of the alternative exon has been reported to enhance alternative splicing and to improve splicing-based riboswitches (51,52). We added a G-quadruplex sequence 18 nucleotides downstream of the aptamer in the best-performing construct (SP_double_anti, see Figure 6A, B). The stable G-quadruplex sequence is originally located in the pre-mRNA sequence of TAF15, a protein involved in mRNA processing in neurons (53–55). The resulting switch (SP_double_anti_GQ) still exhibits reduced exon-skipping in presence of the ligand. However, in absence of oxypurinol, gene expression is even further decreased resulting in an overall improved switching performance of 135-fold induction. When increasing the ligand concentration, we observed an increase in the obtained dynamic range up to 250 fold at a concentration of 5 mM oxypurinol (Figure 6C, assessment of the cell permeability of oxypurinol see Supplementary Note 6).

To validate the mechanism on an RNA level, we performed RT-PCR and qPCR after purifying the RNA from transfected HeLa cells that were cultivated in absence or presence of 2 mM oxypurinol (Supplementary Figure S9, primer sequences are shown in Supplementary Table S5). The results indicate efficient exon skipping in presence of the ligand and low background, as expected. Visualization of the RT-PCR products on an agarose gel reveals a strong band corresponding to the spliced product in the absence of oxypurinol. However, in the presence of oxypurinol, a shorter fragment of approximately 150 bp appears, matching the size of the unspliced sequence. The relative firefly luciferase mRNA abundance was determined via qPCR using primers that bind on the first firefly exon. Similar mRNA levels were observed for the spliced construct and SP_double_anti_GQ in the absence of oxypurinol, while in the presence of oxypurinol, the mRNA levels increased significantly. In order to address the selectivity of triggering the riboswitch, we evaluated a series of purine analogs with regard to concentration-dependent induction of gene expression. Xanthine, oxypurinol and 8-azaxanthine triggered the SP_double_anti_GQ switch, with xanthine and oxypurinol being the most effective inducers, resulting in fold changes of up to 154-fold at 2 mM and 65-fold at 1 mM concentration. With 8-Azaxanthine an induction of ∼80 fold is reached at 2 mM. While addition of allopurinol did not result in a detectable induction, a moderate induction was observed with uric acid(30-fold at 2 mM) and slight induction with hypoxanthine (∼1.8-fold at 2 mM, see Figure 7A, B and Supplementary Figure S11). However, the application of allopurinol and uric acid may cause effects due to slight toxicity within the applied range (Supplementary Figure S10).

We further tested the efficiency of the SP_double_anti_GQ switch in different cell lines and an alternative reporter construct, consisting of mCherry and EGFP (Figure 8). When transfecting with the original luciferase construct, we observed the highest on-switching effect in HeLa cells, which was expected, since the system was optimized in this context. Nevertheless, in HEK293T and H1299 cells, a dynamic range of 40-fold and 56-fold, respectively, could be obtained at 2 mM oxypurinol. When switching to the mCherry-GFP

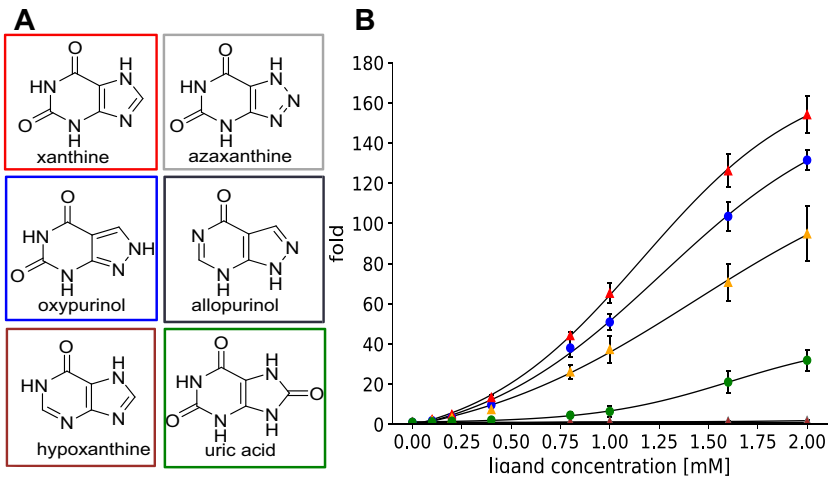

Figure 7. Ligand selectivity of SP_double_anti_GQ. Purine analogs tested for SP_double_anti_GQ induction in HeLa cells. (**A**) Concentration-dependent luciferase expression in HeLa cells under the control of the SP_double_anti_GQ construct upon addition of ligands shown in (**B**): red: xanthine, blue: oxypurinol, grey: azaxanthine, green: uric acid, brown: hypoxanthine, black: allopurinol). Data points represent the mean (±SD) of three independent experiments, performed in triplicates

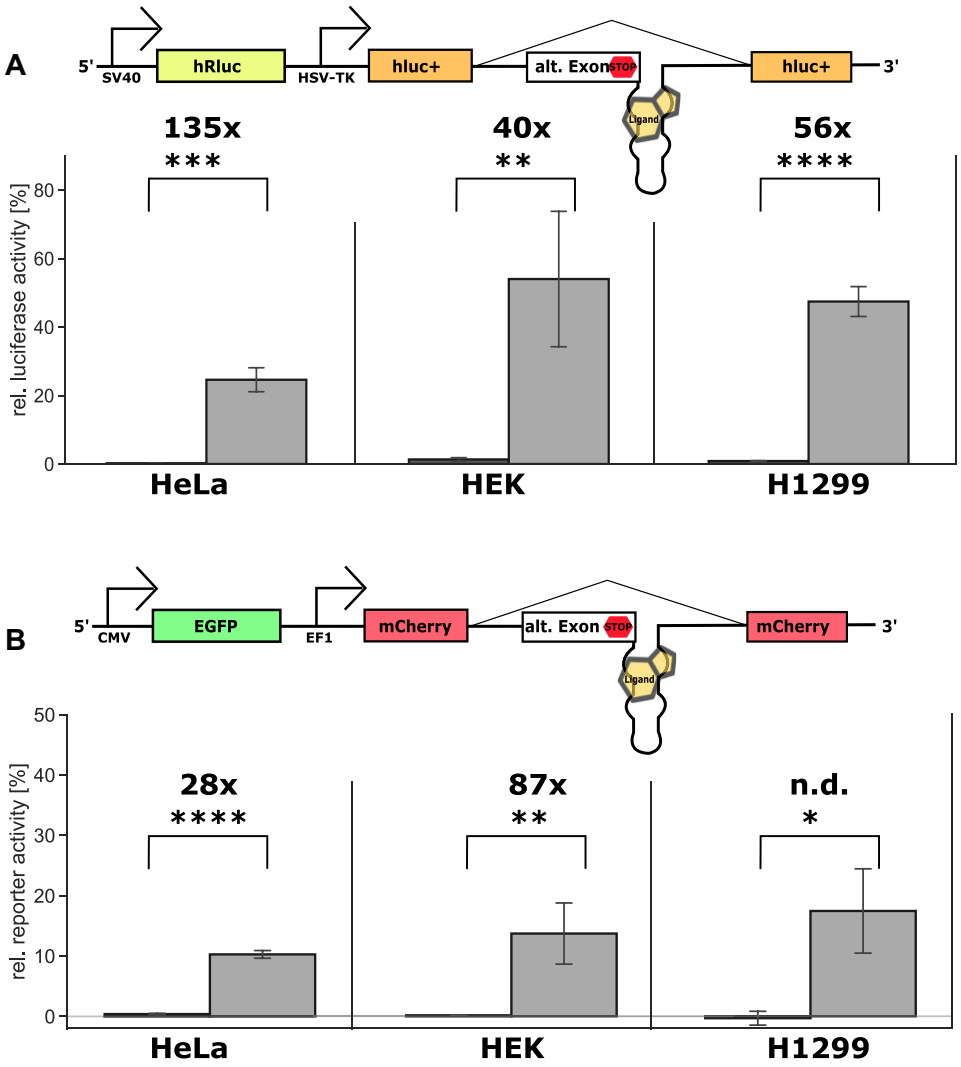

Figure 8. Evaluation of the riboswitch versatility in various cell lines and with different reporter genes. (**A**) HeLa, HEK293T and H1299 cells were transfected with the SP_anti_double_GQ construct, the psiCheck vector and treated with medium with (light grey) or without (dark grey) oxypurinol. (**B**) Evaluation of switching performance in a GFP-mCherry vector with different promotors. Bars represent the mean (±SD) of three independent experiments, performed in triplicates $*P < 0.05$ $**P < 0.01$, $***P < 0.001$.

construct, the measurable efficiency in HEK cells was the highest (87-fold at 2 mM oxypurinol), while the obtained results in HeLa cells were much lower (~28-fold at 2 mM). However, the off-state in this construct was always very close to the background fluorescence and we thus consider the calculated fold change as not very meaningful. In H1299 cells, the dynamic range could not be calculated, since the mean fluorescence in the off-state was lower than the measured background fluorescence. In conclusion, we observed robust switching performances in both other cell lines and with other reporter genes.

Discussion

In this study, we show that the bacterial xanthine I riboswitch binds oxypurinol and is suited for the construction of synthetic RNA switches to control gene expression in human cell lines. Oxypurinol-responsive switches based on a hammerhead ribozyme and alternative splicing platforms were designed and characterized. Splicing-based oxypurinol switches were optimized by introducing a competitor stem, a second aptamer and a quadruplex sequence, ultimately yielding synthetic riboswitches with up to 135-fold induction of gene expression. During the publication process Nomura *et al*. reported the optimization of the AC17–4 riboswitch via competing stems, which proves the transferability of the concept in the context of splicing-based riboswitches (56). Riboswitches enabling efficient protein-independent regulation of gene expression offer new opportunities as tools in basic research, biotechnology as well as future gene therapies. In particular, the last application requires riboswitch systems that are triggered by ligands that have favorable pharmacological properties for human use.

Prior to this work, mostly tetracycline aptamers have been employed for the design of riboswitches in eukaryotic expression systems and model organisms such as in human cells, *C. elegans* and mice (9,20,42,57). Combinations of tetracycline aptamers with exon-skipping expression platforms allow effective regulation (42). Recently, a highly optimized tetracycline switch system was reported by placing a polyA-signal into a Y-shaped scaffold made up by three aptamers that additionally control a G-quadruplex-assisted splice site (52). However, the antibiotic activity of tetracycline poses the risk of side effects and the development of antibiotic resistance. Strategies for the development of riboswitches responsive to more favorable ligands mainly focused on the implementation of *in vitro*-selected aptamers (58).

Consideration of naturally occurring aptamers, which have been optimized by evolution to bind their cognate ligands with high affinity and selectivity, holds promise for expanding the available repertoire of ligand sensing aptamer domains. Notably, some bacterial riboswitches exhibit a responsiveness to non-natural derivatives of their cognate ligands that sometimes results in an antibiotic effect (59–61). For example, the thiamine pyrophosphate (TPP) riboswitch is also triggered by derivatives such as pyrithiamine (62,60). We exploit a previously unrecognized promiscuity of the natural xanthine aptamer. The switches developed here have been optimized to a level that shows initial induction of gene expression at approximately 100–250 μM oxypurinol (Figure 6). Comparable serum/plasma concentrations of oxypurinol have been reported in patients treated for hyperuricemia (63,64). Nevertheless, for potential uses in therapeutic applications the presented switches will need further optimization due to the moderate fold changes within this range. The natural riboswitch ligand xanthine occurs as an endogenous metabolite in purine catabolism (Supplementary Scheme 1). However, xanthine levels are usually <2 μM (65). Thus, intracellular levels of xanthine are not expected to reach concentrations that trigger the presented riboswitches. In addition, the affinities of uric acid and hypoxanthine for the xanthine I riboswitch aptamer are comparably low (30) and did not trigger pronounced induction of gene expression at physiological concentrations(Figure 6A). By employing a well-known, nontoxic and non-antibiotic drug, the switches developed in this study offer robust and efficient tools for the mammalian synthetic biology community, enabling precise cellular applications without adversely affecting cell viability. Although the synthetic oxypurinol-inducible RNA switches appear to be selective, applications in therapeutic approaches require optimization in order to achieve higher sensitivities, i.e. more stringent induction of gene expression at lower oxypurinol concentrations.

Data availability

The data underlying this article are available in the PDB at https://www.rcsb.org/ and can be accessed with accession number 8Q6N. Other data and materials are available upon request.

Supplementary data

Supplementary Data are available at NAR Online.

Acknowledgements

The authors thank Astrid Joachimi, Dmitry Galetskyi (University of Konstanz), Yvette Hoevels and Stefanie Gruber (Boehringer Ingelheim Pharma GmbH & Co. KG) for excellent technical assistance.

Funding

Funding for open access charge: University of Konstanz, AG Hartig.

Conflict of interest statement

H.N., G.S., H.K., D.G., G.A., M.K. are employees of Boehringer Ingelheim.

References

1. Mandal,M., Boese,B., Barrick,J.E., Winkler,W.C. and Breaker,R.R. (2003) Riboswitches control fundamental biochemical pathways in Bacillus subtilis and other bacteria. *Cell*, **113**, 577–586.
2. Kallunki,T., Barisic,M., Jäättelä,M. and Liu,B. (2019) How to choose the right inducible gene expression system for mammalian studies? *Cells*, **8**, 796.
3. Tickner,Z.J. and Farzan,M. (2021) Riboswitches for controlled expression of therapeutic transgenes delivered by adeno-associated viral vectors. *Pharmaceuticals*, **14**, 554.
4. Mandal,M. and Breaker,R.R. (2004) Gene regulation by riboswitches. *Nat. Rev. Mol. Cell Biol.*, **5**, 451–463.

5. Winkler,W.C. and Breaker,R.R. (2005) Regulation of bacterial gene expression by riboswitches. *Annu. Rev. Microbiol.*, **59**, 487–517.
6. Sack,M., Stifel,J., Kreft,S.G., Deuerling,E. and Hartig,J.S. (2019) Neomycin-dependent hammerhead ribozymes for the direct control of gene expression in Saccharomyces cerevisiae. *Methods*, **161**, 35–40.
7. Beilstein,K., Wittmann,A., Grez,M. and Suess,B. (2015) Conditional control of mammalian gene expression by tetracycline-dependent hammerhead ribozymes. *ACS Synth. Biol.*, **4**, 526–534.
8. Mustafina,K., Nomura,Y., Rotrattanadumrong,R. and Yokobayashi,Y.J.A.S.B. (2021) Circularly-permuted pistol ribozyme: a synthetic ribozyme scaffold for mammalian riboswitches. **10**, 2040–2048.
9. Spöring,M., Boneberg,R. and Hartig,J.S. (2020) Aptamer-mediated control of polyadenylation for gene expression regulation in mammalian cells. *ACS Synth. Biol.*, **9**, 3008–3018.
10. Zhong,G., Wang,H., Bailey,C.C., Gao,G. and Farzan,M. (2016) Rational design of aptazyme riboswitches for efficient control of gene expression in mammalian cells. *eLife*, **5**, e18858.
11. Bell,C.L., Yu,D., Smolke,C.D., Geall,A.J., Beard,C.W. and Mason,P.W. (2015) Control of alphavirus-based gene expression using engineered riboswitches. *Virology*, **483**, 302–311.
12. Berens,C., Thain,A. and Schroeder,R. (2001) A tetracycline-binding RNA aptamer. *Bioorg. Med. Chem.*, **9**, 2549–2556.
13. Vogel,M., Weigand,J.E., Kluge,B., Grez,M. and Suess,B. (2018) A small, portable RNA device for the control of exon skipping in mammalian cells. *Nucleic Acids Res.*, **46**, e48.
14. Wurmthaler,L.A., Sack,M., Gense,K., Hartig,J.S. and Gamerdinger,M. (2019) A tetracycline-dependent ribozyme switch allows conditional induction of gene expression in Caenorhabditis elegans. *Nat. Commun.*, **10**, 491.
15. Strobel,B., Düchs,M.J., Blazevic,D., Rechtsteiner,P., Braun,C., Baum-Kroker,K.S., Schmid,B., Ciossek,T., Gottschling,D., Hartig,J.S., *et al.* (2020) A Small-Molecule-Responsive Riboswitch Enables Conditional Induction of Viral Vector-Mediated Gene Expression in Mice. *ACS Synth. Biol.*, **9**, 1292–1305.
16. Ketzer,P., Kaufmann,J.K., Engelhardt,S., Bossow,S., Von Kalle,C., Hartig,J.S., Ungerechts,G. and Nettelbeck,D.M. (2014) Artificial riboswitches for gene expression and replication control of DNA and RNA viruses. *Proc. Natl. Acad. Sci. U.S.A.*, **111**, E554–E562.
17. Zhong,G., Wang,H., He,W., Li,Y., Mou,H., Tickner,Z.J., Tran,M.H., Ou,T., Yin,Y. and Diao,H. (2020) A reversible RNA on-switch that controls gene expression of AAV-delivered therapeutics in vivo. *Nat. Biotechnol.*, **38**, 169–175.
18. Eriksson,R.A.E., Nieminen,T., Galibert,L., Peltola,S.K., Tikkanen,P., Käyhty,P., Leinonen,H.M., Oruetxebarria,I., Lepola,S. and Valkama,A.J. (2022) Optimized riboswitch-regulated AAV vector for VEGF-B gene therapy. *Front. Med.*, **9**, 1052318.
19. Mou,H., Zhong,G., Gardner,M.R., Wang,H., Wang,Y.-W., Cheng,D. and Farzan,M. (2018) Conditional regulation of gene expression by ligand-induced occlusion of a MicroRNA target sequence. *Mol. Ther.*, **26**, 1277–1286.
20. Düchs,M.J., Kratzer,R.F., Vieyra-Garcia,P., Strobel,B., Schönberger,T., Groß,P., Aljayyoussi,G., Gupta,A., Lang,I. and Klein,H. (2024) Riboswitch-controlled IL-12 gene therapy reduces hepatocellular cancer in mice. *Front. Immunol.*, **15**, 1360063.
21. Nomura,Y., Zhou,L., Miu,A. and Yokobayashi,Y. (2013) Controlling mammalian gene expression by allosteric hepatitis delta virus ribozymes. *ACS Synth. Biol.*, **2**, 684–689.
22. Hötzel,J. and Suess,B. (2022) Structural changes in aptamers are essential for synthetic riboswitch engineering. *J. Mol. Biol.*, **434**, 167631.
23. Lotz,T.S. and Suess,B. (2018) Small-molecule-binding riboswitches. *Microbiol. Spectr.*, **6**, 6–4.
24. Stifel,J., Spöring,M. and Hartig,J.S. (2019) Expanding the toolbox of synthetic riboswitches with guanine-dependent aptazymes. *Synth. Biol.*, **4**, ysy022.
25. Townshend,B., Kaplan,M. and Smolke,C.D. (2022) Highly multiplexed selection of RNA aptamers against a small molecule library. *PLoS One*, **17**, e0273381.
26. Kraus,L., Duchardt-Ferner,E., Bräuchle,E., Fürbacher,S., Kelvin,D., Marx,H., Boussebayle,A., Maurer,L.-M., Bofill-Bosch,C. and Wöhnert,J. (2023) Development of a novel tobramycin dependent riboswitch. *Nucleic Acids Res.*, **51**, 11375–11385.
27. Fukunaga,K., Dhamodharan,V., Miyahira,N., Nomura,Y., Mustafina,K., Oosumi,Y., Takayama,K., Kanai,A. and Yokobayashi,Y. (2023) Small-molecule aptamer for regulating RNA functions in mammalian cells and animals. *J. Am. Chem. Soc.*, **145**, 7820–7828.
28. Mulhbacher,J., Brouillette,E., Allard,M., Fortier,L.-C., Malouin,F. and Lafontaine,D.A. (2010) Novel riboswitch ligand analogs as selective inhibitors of guanine-related metabolic pathways. *PLoS Pathog.*, **6**, e1000865.
29. Kim,J.N., Blount,K.F., Puskarz,I., Lim,J., Link,K.H. and Breaker,R.R. (2009) Design and antimicrobial action of purine analogues that bind guanine riboswitches. *ACS Chem. Biol.*, **4**, 915–927.
30. Yu,D. and Breaker,R.R. (2020) A bacterial riboswitch class senses xanthine and uric acid to regulate genes associated with purine oxidation. *RNA*, **26**, 960–968.
31. Weinberg,Z., Lünse,C.E., Corbino,K.A., Ames,T.D., Nelson,J.W., Roth,A., Perkins,K.R., Sherlock,M.E. and Breaker,R.R. (2017) Detection of 224 candidate structured RNAs by comparative analysis of specific subsets of intergenic regions. *Nucleic Acids Res.*, **45**, 10811–10823.
32. Hamal Dhakal,S., Panchapakesan,S. S., Slattery,P., Roth,A. and Breaker,R. R. (2022) Variants of the guanine riboswitch class exhibit altered ligand specificities for xanthine, guanine, or 2′-deoxyguanosine. *Proc. Natl. Acad. Sci. USA*, **119**, e2120246119.
33. Xu,X., Egger,M., Chen,H., Bartosik,K., Micura,R. and Ren,A. (2021) Insights into xanthine riboswitch structure and metal ion-mediated ligand recognition. *Nucleic Acids Res.*, **49**, 7139–7153.
34. Buchanan,J.M. (1960) Biosynthesis of purine nucleotides. *Nucleic Acids*, **3**, 303–322.
35. Taniguchi,A. and Kamatani,N. (2008) Control of renal uric acid excretion and gout. *Curr. Opin. Rheumatol.*, **20**, 192–197.
36. Day,R.O., Graham,G.G., Hicks,M., McLachlan,A.J., Stocker,S.L. and Williams,K.M. (2007) Clinical pharmacokinetics and pharmacodynamics of allopurinol and oxypurinol. *Clin. Pharmacokinet.*, **46**, 623–644.
37. Rundles,R.W., Metz,E.N. and Silberman,H.R. (1966) Allopurinol in the treatment of gout. *Ann. Intern. Med.*, **64**, 229–258.
38. Kane,S.P. (2021) ClinCalc DrugStats Database (Version 2021). *ClinCalc*. https://clincalc.com.
39. WHO Model List of Essential Medicines - 23rd list (2023) *WHO/MHP/HPS/EML/2023.02*. World Health Organization, Geneva.
40. Lenkeit,F., Eckert,I., Hartig,J.S. and Weinberg,Z. (2020) Discovery and characterization of a fourth class of guanidine riboswitches. *Nucleic Acids Res.*, **48**, 12889–12899.
41. Soukup,G.A. and Breaker,R.R. (1999) Relationship between internucleotide linkage geometry and the stability of RNA. *RNA*, **5**, 1308–1325.
42. Finke,M., Brecht,D., Stifel,J., Gense,K., Gamerdinger,M. and Hartig,J.S. (2021) Efficient splicing-based RNA regulators for tetracycline-inducible gene expression in human cell culture and C. elegans. *Nucleic Acids Res.*, **49**, e71.
43. Emsley,P. and Cowtan,K. (2004) Coot: model-building tools for molecular graphics. *Acta Crystallogr. Sect. D Biol. Crystallogr.*, **60**, 2126–2132.

44. Bricogne,G.B.E., Brandl,M., Flensburg,C., Keller,P., Paciorek,W., Roversi,P., Sharff,A., Smart,O.S., Vonrhein,C., *et al.* (2017) *BUSTER version 2.11.8*. Global Phasing Ltd, Cambridge, United Kingdom.
45. Jolley,E.A. and Znosko,B.M. (2017) The loss of a hydrogen bond: thermodynamic contributions of a non-standard nucleotide. *Nucleic Acids Res.*, **45**, 1479–1487.
46. Felletti,M., Stifel,J., Wurmthaler,L.A., Geiger,S. and Hartig,J.S. (2016) Twister ribozymes as highly versatile expression platforms for artificial riboswitches. *Nat. Commun.*, **7**, 12834.
47. Ceres,P., Garst,A.D., Marcano-Velázquez,J.G. and Batey,R.T. (2013) Modularity of select riboswitch expression platforms enables facile engineering of novel genetic regulatory devices. *ACS Synth. Biol.*, **2**, 463–472.
48. Wieland,M., Benz,A., Klauser,B. and Hartig,J.S. (2009) Artificial ribozyme switches containing natural riboswitch aptamer domains. *Angew. Chem. Int. Ed.*, **48**, 2715–2718.
49. Boyne,A.R., Danos,O.F., Volles,M.J. and Guo,X. (2019) *Regulation of gene expression by aptamer-mediated modulation of alternative splicing*. Google Patents.
50. Tucker,B.J. and Breaker,R.R. (2005) Riboswitches as versatile gene control elements. *Curr. Opin. Struct. Biol.*, **15**, 342–348.
51. Georgakopoulos-Soares,I., Parada,G.E., Wong,H.Y., Medhi,R., Furlan,G., Munita,R., Miska,E.A., Kwok,C.K. and Hemberg,M. (2022) Alternative splicing modulation by G-quadruplexes. *Nat. Commun.*, **13**, 2404.
52. Luo,L., Jea,J.D.-Y., Wang,Y., Chao,P.-W. and Yen,L. (2024) Control of mammalian gene expression by modulation of polyA signal cleavage at 5′ UTR. *Nat. Biotechnol.*, **42**, 1454–1466.
53. Pandey,S., Agarwala,P. and Maiti,S. (2013) Effect of loops and G-quartets on the stability of RNA G-quadruplexes. *J. Phys. Chem. B*, **117**, 6896–6905.
54. Ibrahim,F., Maragkakis,M., Alexiou,P., Maronski,M.A., Dichter,M.A. and Mourelatos,Z. (2013) Identification of in vivo, conserved, TAF15 RNA binding sites reveals the impact of TAF15 on the neuronal transcriptome. *Cell Rep.*, **3**, 301–308.
55. Lee,D.S.M., Ghanem,L.R. and Barash,Y. (2020) Integrative analysis reveals RNA G-quadruplexes in UTRs are selectively constrained and enriched for functional associations. *Nat. Commun.*, **11**, 527.
56. Nomura,Y., Kim,N., Zhu,B., Hamzah,M., Zhang,H. and Yokobayashi,Y. (2024) Optimization of Exon-Skipping Riboswitches and Their Applications to Control Mammalian Cell Fate. *ACS Synth. Biol.*, **13**, 3246–3255.
57. Strobel,B., Düchs,M.J., Blazevic,D., Rechtsteiner,P., Braun,C., Baum-Kroker,K.S., Schmid,B., Ciossek,T., Gottschling,D. and Hartig,J.r.S. (2020) A small-molecule-responsive riboswitch enables conditional induction of viral vector-mediated gene expression in mice. *ACS Synth. Biol.*, **9**, 1292–1305.
58. Boussebayle,A., Torka,D., Ollivaud,S., Braun,J., Bofill-Bosch,C., Dombrowski,M., Groher,F., Hamacher,K. and Suess,B. (2019) Next-level riboswitch development—implementation of Capture-SELEX facilitates identification of a new synthetic riboswitch. *Nucleic Acids Res.*, **47**, 4883–4895.
59. Panchal,V. and Brenk,R. (2021) Riboswitches as drug targets for antibiotics. *Antibiotics*, **10**, 45.
60. Sudarsan,N., Cohen-Chalamish,S., Nakamura,S., Emilsson,G.M. and Breaker,R.R.J.C. (2005) biology, Thiamine pyrophosphate riboswitches are targets for the antimicrobial compound pyrithiamine. **12**, 1325–1335.
61. Gilbert,S.D., Reyes,F.E., Edwards,A.L. and Batey,R.T. (2009) Adaptive ligand binding by the purine riboswitch in the recognition of guanine and adenine analogs. *Structure*, **17**, 857–868.
62. Wakchaure,P.D. and Ganguly,B. (2023) Exploring the structure, function of thiamine pyrophosphate riboswitch and designing small molecules for antibacterial activity. *Wiley Interdiscipl. Rev. RNA*, **14**, e1774.
63. Stamp,L.K., Barclay,M.L., O'Donnell,J.L., Zhang,M., Drake,J., Frampton,C. and Chapman,P.T. (2011) Relationship between serum urate and plasma oxypurinol in the management of gout: determination of minimum plasma oxypurinol concentration to achieve a target serum urate level. *Clin. Pharmacol. Ther.*, **90**, 392–398.
64. Wright,D.F.B., Stamp,L.K., Merriman,T.R., Barclay,M.L., Duffull,S.B. and Holford,N.H.G. (2013) The population pharmacokinetics of allopurinol and oxypurinol in patients with gout. *Eur. J. Clin. Pharmacol.*, **69**, 1411–1421.
65. Furuhashi,M., Koyama,M., Higashiura,Y., Murase,T., Nakamura,T., Matsumoto,M., Sakai,A., Ohnishi,H., Tanaka,M. and Saitoh,S. (2020) Differential regulation of hypoxanthine and xanthine by obesity in a general population. *J. Diabetes Invest.*, **11**, 878–887.

Received: May 15, 2024. **Revised:** September 24, 2024. **Editorial Decision:** October 24, 2024. **Accepted:** February 19, 2025